Medical Volume Segmentation based on Level Sets of Probabilities

Yugang Liu[1] and Yizhou Yu[2]
[1]*Department of Computer Science and Engineering,*
University of Electronic Science and Technology of China, Chengdu, China
[2]*University of Illinois at Urbana-Champaign, Illinois, U.S.A.*

Keywords: Medial Image Segmentation, Level Set Method, Discriminative Probabilistic Classifier.

Abstract: In this paper, we present a robust and accurate method for biomedical image segmentation using level sets of probabilities. The level set method is a popular technique in biomedical image segmentation. Our method integrates a probabilistic classifier with the level set method, making the level set method less vulnerable to local minima. Given the local attributes within a neighborhood of a voxel, this classifier outputs an estimated likelihood of the voxel being part of an object of interest. Our method obtains a posterior probabilistic mask of the object of interest according to such estimated likelihoods, an edge field and a smoothness prior. We further alternate classifier training and the level set method to improve the performance of both. We have successfully applied our method to the segmentation of various organs and tissues in the Visible Human dataset. Experiments and comparisons demonstrate our method can accurately extract volumetric objects of interest, and outperforms traditional levelset-based segmentation algorithms.

1 INTRODUCTION

The growing size and number of these medical images have necessitated the use of computers to facilitate processing and analysis. In particular, computer algorithms for the delineation of anatomical structure and other regions of interest are becoming increasingly important in assisting and automating specific radiological tasks (Pham et al., 2000). Three-dimensional segmentation of biomedical volumetric image data, a foundation of high-level medical image analysis, has important significance in biomedical engineering.

The level set method (LSM) is a popular technique in biomedical image segmentation. This is due to many reasons. LSM represents the segmentation boundary in an implicit and parameter-free way, which is convenient for checking whether points belong to the interior of the segmented region. The implicit representation is also particularly convenient for evolving the topology of the segmentation boundary during a solution process. Furthermore, LSM can be used to define a generic optimization framework. All sorts of criteria judging the quality of a segmentation can be integrated into this framework as priors. Thus solving this generic optimization can be cast as solving the PDE of the level set method.

Nevertheless, a serious limitation of many existing level set algorithms for image segmentation is that the final result is very sensitive to the location of the initialization. This is because the above optimization typically has many local minima to trap level set evolution, which is driven by forces computed from local image data in the vicinity of the zero level set.

In this paper, we present an interactive volume image segmentation technique that overcomes this limitation. This technique generalizes the 2D image segmentation algorithm presented in (Liu and Yu, 2012), which integrates a discriminative classifier with the level set method. The classifier performs pixelwise classification over the entire image domain and feeds information garnered during this process to the level set method, which thus gains a more "global" understanding regarding which local image regions likely belong to an object of interest.

However, generalizing the 2D segmentation algorithm in (Liu and Yu, 2012) to volume images imposes a few challenges. First, volume images typically have less color and texture variations. It is unclear how to define effective volume texture descriptors and volume edges which provide important information to the classifier as well as the level set method. Second, the number of voxels in a volume image is much larger than the number of pixels in a 2D image. It is unclear how to perform voxelwise classification in a reasonably efficient way while still guarantee a high classification accuracy.

Liu Y. and Yu Y..
Medical Volume Segmentation based on Level Sets of Probabilities.
DOI: 10.5220/0004185903870394
In *Proceedings of the International Conference on Computer Vision Theory and Applications* (VISAPP-2013), pages 387-394
ISBN: 978-989-8565-47-1

In summary, the contributions of this paper are as follows.

- We generalize the weakly supervised levelset-based 2D image segmentation framework in (Liu and Yu, 2012) to three-dimensional volume images. Experiments and comparisons indicate this generalized algorithm can accurately extract volumetric objects of interest without the assistance of a shape prior, and outperforms the graphcut algorithm and traditional levelset-based algorithms on volume images.
- In our generalized algorithm, we adopt a boosted logistic classifier as the probabilistic classifier integrated with the level set method. In comparison with other boosted classifiers, this one can be evaluated efficiently on new testing data while maintaining comparable classification accuracy.
- We also extend 2D edge and texture feature extraction to 3D volume images.

2 BACKGROUND AND RELATED WORK

In this section we review previous segmentation techniques and focus on level set methods for biomedical images. The majority of previous work on levelset based image segmentation is unsupervised except for (Paragios and Deriche, 1999; Liu and Yu, 2012), where a user can provide hints by drawing boxes or a convex hull over the foreground object. In comparison with the interactive segmentation method in this paper, the work in (Paragios and Deriche, 1999) only adopts a relatively simple statistical model and does not consider distant interactions with edge pixels. As a result, region boundaries are often trapped in local minima, and do not snap to true object boundaries. A state-of-the-art levelset based technique for interactive segmentation of 2D natural images has been presented in (Liu and Yu, 2012), where the level set method is integrated with a discriminative probabilistic classifier and carefully designed features are used for differentiating textures. In this paper, we generalize the method in (Liu and Yu, 2012) to volumetric biomedical images.

A method for segmenting thin structures has been presented in (Holtzman-Gazit et al., 2006), which integrates edge information with the minimal variance criterion for segmented regions. However, the minimal variance criterion is a simple classifier that cannot cope with complex textures in medical images. Because of its unsupervised nature, the presented results in this paper do not have very accurate object boundaries. A method for segmenting brain tumor in MRI images has been presented in (Cobzas et al., 2007). However, this approach has to learn a statistical model for tumor and normal tissue using manually segmented data. A method for segmenting medical images using hybrid discriminative/generative models has been presented in (Tu et al., 2008). This method integrates a discriminative classifier with a generative shape model. Region boundary evolution based on this hybrid model is performed using the level set method. However, this approach is still a region-growing method and cannot handle objects with a complex topology very well.

3 OVERVIEW

The key idea of level sets of probabilities is to integrate a probabilistic voxel classifier with the level set method, making the level set method less vulnerable to local minima. Given the attributes within a neighborhood of a voxel, this classifier outputs an estimated likelihood of the voxel being part of an object of interest. Our goal is to obtain a voxelwise posterior probability based on this estimated likelihood and certain prior models of the object of interest. To integrate the classifier with the level set method, we attempt to make a transformed version of the level set function, $\Phi(\mathbf{x},t)$, achieve an increasingly better approximation of a posterior probabilistic mask of the object of interest over time. Since probabilities fall into $[0,1]$ while the values of our level set function belong to $[-1,1]$ with positive values falling outside the zero level set, a voxelwise probabilistic mask needs to be transformed as follows to become a level set function:

$$\Phi(\mathbf{x}) = -2(P(l(\mathbf{x}) = 1|I) - 0.5), \qquad (1)$$

where $l(\mathbf{x})$ denotes the label of voxel $\mathbf{x}$, and $P(l(\mathbf{x}) = 1|I)$ represents the posterior probability of voxel $\mathbf{x}$ being part of the object of interest. Generally speaking, there are few necessary conditions if any that a level set function has to satisfy except that Lipschitz continuity is a desired property for sampling and numerical approximation (Osher and Fedkiw, 2003). Since the probability values at two adjacent voxels can at most differ by one, our level set function by default has Lipschitz continuity. In practice, we also apply low-pass filtering to the latest level set function at the end of each time step to make it smoother.

Since our method belongs to supervised level set methods, it requires a small amount of user interaction. The user can simply draw 3D boxes around local regions in the object of interest as well as in the background (Fig. 1(b)). Given initial user-supplied boxes,

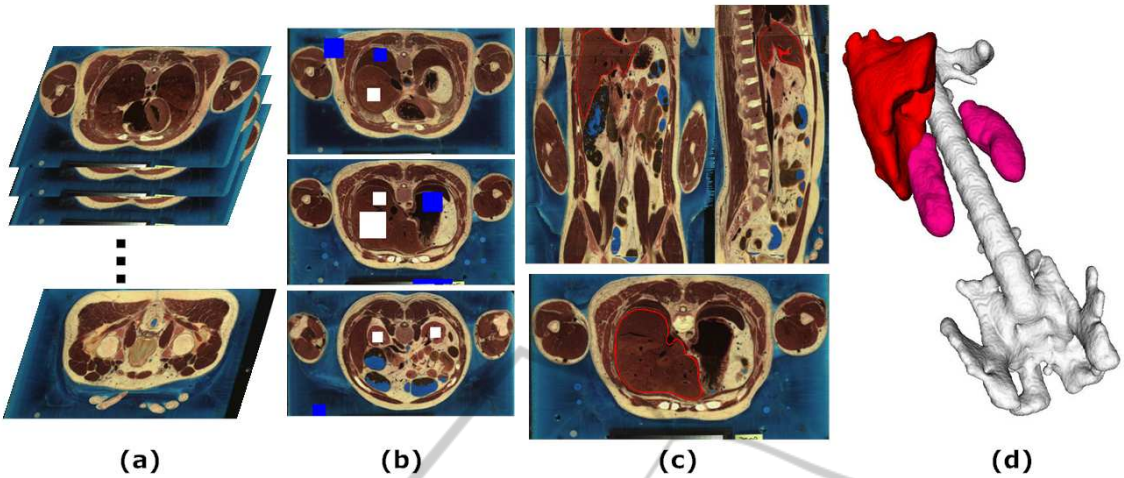

Figure 1: The pipeline of our method. (a) Biomedical volumetric image data, (b) initial user-drawn regions (white for object, blue for background), (c) the final segmentation result (red curve is the zero level set), (d) 3D visualization (white for spine, pink for kidneys, red for liver).

a probabilistic voxel classifier can be trained. And the level set function is initialized according to voxel-wise likelihoods estimated by the probabilistic classifier. Once initialized, we run the level set method until it converges to obtain a mask of the object of interest. Note that we can alternate classifier training and the level set method to improve the performance of both.

Fig. 2 shows a comparison of the results that can be achieved with traditional level set methods and our new method. Obviously, a traditional level set method can easily return a local minimum as a solution, which omits the white matter on the left cerebral hemisphere in the image. In contrast, all the white matter can be extracted with our algorithm.

Figure 2: Comparison of segmented white matter in a medical image. (a) Initial user-drawn white rectangle, (b) segmentation result from a traditional level set method, (c) segmentation result from our revised level set method.

4 LEVEL SETS OF PROBABILITIES

Our level set method tracks the evolution of the front by numerically solving the following differential equation and extracting the zero level set of the solution:

$$\frac{\partial \Phi}{\partial t} = -\left[\underbrace{\alpha \cdot R(\mathbf{x},t)}_{\text{classifier}} + \underbrace{\beta \cdot B(\mathbf{x},t)}_{\text{edge field}} + \underbrace{\gamma \cdot C(\mathbf{x},t)}_{\text{curvature}}\right] \|\nabla \Phi\|, \tag{2}$$

where $\mathbf{x}$ denotes voxel coordinates in the image and t denotes the time of advection. In (2), the evolution of the zero level set is driven by three force terms, the *classifier force*, *edge field force*, and *curvature force*, which will be briefly discussed below as they are adapted from the force terms in (Liu and Yu, 2012).

The equation in (2) can be efficiently solved using the narrow band method in (Sethian, 1999; Osher and Fedkiw, 2003) and the fast local level set method in (Peng et al., 1999).

• Classifier Force. We define the following energy term E_R to measure the degree of inconsistency between global posterior probabilities and local likelihoods returned by the voxel classifier:

$$E_R = \iiint_I \left(\Phi(\mathbf{x}) - \Phi^0(\mathbf{x})\right)^2 d\mathbf{x}, \tag{3}$$

where $\Phi^0(\mathbf{x}) = -2(P(l(\mathbf{x}) = 1|N(\mathbf{x})) - 0.5)$, where $P(l(\mathbf{x}) = 1|N(\mathbf{x}))$ denotes the likelihood of voxel $\mathbf{x}$ being part of the object of interest according to the probabilistic classifier, which only gathers evidences available from a local neighborhood $N(\mathbf{x})$. By taking the derivative of (3) with respect to the level set passing through $\mathbf{x}$, we obtain the following force term that reduces the energy in (3):

$$R(\mathbf{x})\frac{\nabla \Phi}{\|\nabla \Phi\|} = \left(\Phi(\mathbf{x}) - \Phi^0(\mathbf{x})\right)\frac{\nabla \Phi}{\|\nabla \Phi\|}, \tag{4}$$

where $\frac{\nabla\Phi}{\|\nabla\Phi\|}$ represents the unit outward normal vector of the zero level set.

• Edge Field Force. A second goal is to make the zero level set snap to salient edges in the volume image because salient edges are likely to lie on the boundary surface of the object of interest. This is achieved with an unsigned distance transform of salient edge voxels, $\Psi(\mathbf{x})$. We adopt the following energy term E_B to measure the overall proximity between the zero level set and the set of salient edges:

$$E_B(\Omega) = \oiint_{\Omega} \Psi(\mathbf{x}(u,v)) \, \|\Omega_u \times \Omega_v\| \, du dv, \quad (5)$$

where $\Omega(u,v)$ is a 2D parametrization of the zero level set, and $u \in [0,1]$, $v \in [0,1]$, respectively. $\mathbf{x} : \Omega \to I$ is a mapping from parametric coordinates to 3D image coordinates.

With such an energy term in mind, we define the second force term for boundary localization as follows:

$$B(\mathbf{x})\frac{\nabla\Phi}{\|\nabla\Phi\|} = -\left(\nabla\Psi(\mathbf{x}) \cdot \frac{\nabla\Phi(\mathbf{x})}{\|\nabla\Phi(\mathbf{x})\|}\right)\frac{\nabla\Phi}{\|\nabla\Phi\|}, \quad (6)$$

which tries to move the zero level set towards salient edges by following the negative gradient of the edge field.

• Curvature Force. The curvature force is a standard term in level set methods. Our curvature force tries to provide a tradeoff between boundary smoothness and boundary faithfulness. That means in the vicinity of edges, boundary localization is still a more important goal than boundary smoothness. But in the absence of edges, boundary smoothness serves as an effective prior to determine the shape and position of the local object boundary. We define the curvature force as follows:

$$C(\mathbf{x})\frac{\nabla\Phi}{\|\nabla\Phi\|} = -(\mu\kappa(\mathbf{x}) + (1-\mu)\Psi(\mathbf{x})\kappa(\mathbf{x}))\frac{\nabla\Phi}{\|\nabla\Phi\|}, \quad (7)$$

where $\kappa(\mathbf{x})$ denotes the mean curvature of the level set surface passing through $\mathbf{x}$, and $0 \le \mu \le 1$. The second term in (7) modulates curvature with the edge field to weaken the curvature force in the vicinity of edges. Nevertheless, the first term guarantees that the curvature force does not disappear completely as long as μ remains positive. A formula for the mean curvature of the zero level set in a three-dimensional space can be found in (Osher and Fedkiw, 2003),

The evolution of the zero level set driven by the force in (2) is illustrated in Fig. 3. The initial zero level set is fragmented because of the noisy voxelwise likelihoods from the classifier. Note that although being fragmented, these contours spread over the entire object, making the level set method less likely to be stuck in local minima. These initial contours are evolved by the level set method. They gradually merge with each other and also move toward true object boundaries to improve their localization and spatial coherence. Thus, our segmentation algorithm can also be viewed as an advanced version of region-split-and-merge algorithms.

4.1 Discriminative Probabilistic Classifier

Our level set method relies on the accuracy of the voxel classifier. Logistic regression can serve as a probabilistic classifier. To further improve the accuracy of logistic regression, we adopt the LogitBoost model in (Friedman et al., 2000) as the classifier. This logistic boosting model is a discriminative model and it is well known in machine learning that discriminative models in general can achieve better classification performance than generative models (Tu et al., 2008). In addition, a significant advantage that LogitBoost has over other probabilistic boosting models is that it has relatively few nodes and can be constructed efficiently (Friedman et al., 2000), making it more suitable for large-scale data mining applications.

The input to the classifier consists of 3 color channels and Gabor filter responses. Oriented filter banks have proven to be an effective method to characterize textures (Manjunath and Ma, 1996). We primarily use local statistics of oriented filter responses to differentiate textures. We extend Gabor filtering to volume images by performing 2D Gabor filtering respectively in the X-Y, Y-Z and Z-X cross sections of the volumetric neighborhood of a voxel. We apply 24 Gabor filters (Manjunath and Ma, 1996) at 6 orientations and 4 scales at every voxel in the grayscale version of the image, and such filtering is performed on three orthogonal cross sections, respectively. Thus, every voxel has a 72-component filter response vector.

4.2 3D Edge Field

We perform 3D edge detection before the construction of the 3D edge field. We generalize the principles of traditional 2D Canny edge detection to 3D spaces. An edge in a 2D image is a curve while it becomes a surface in a 3D volume image. In this paper, we use 3D Sobel kernel (Hadwiger et al., 2006) to compute the gradient of every voxel and rely on non-maximum suppression to detect 3D Canny edges in a volume image. For color volume images, we need to convert them to grayscale images before edge detection is performed. We either use the traditional color-to-grayscale conversion or the PCA-based conversion

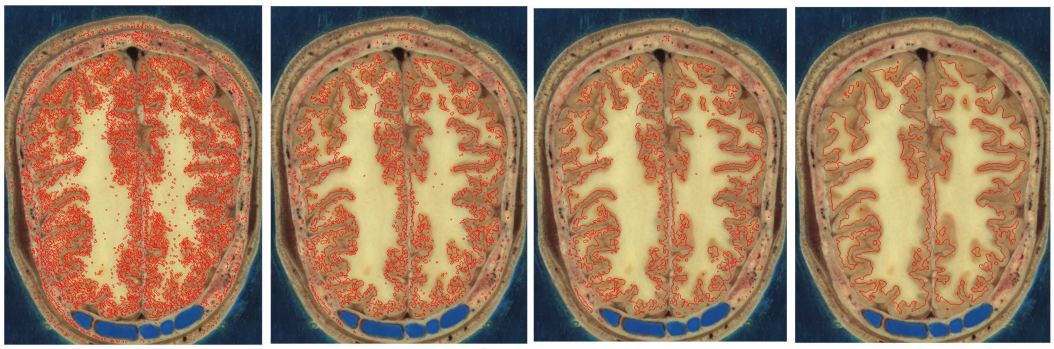

Figure 3: The evolution of our revised zero level sets. (a) An initial zero level set initialized by the probabilistic classifier, (b) an updated zero level set at time step 1, (c) an updated zero level set at time step 2, (d) final pixelwise posterior probabilities.

proposed in (Liu and Yu, 2012).

To make the zero level set quickly snap to salient edges without being trapped in local minima, a global mechanism is needed to facilitate distant interactions between detected edges and level sets. A simple method to achieve this goal is to compute a distance transform of the edges. Since edges are not closed surfaces, we cannot compute a signed distance transform. Instead, we compute an unsigned distance transform using a revised version of the fast marching method in (Sethian, 1999). We further clamp and normalize the distances using a prescribed maximal distance, d_{max} [1]. The result is called an *edge field*, $\Psi(\mathbf{x})$.

$$\Psi(\mathbf{x}_i) = \begin{cases} 0 & \text{for} \quad \mathbf{x}_i \in S_e; \\ \frac{\min(d_{max}, \min_{\mathbf{x}_j \in S_e} d(\mathbf{x}_i, \mathbf{x}_j))}{d_{max}} & \text{for} \quad \mathbf{x}_i \notin S_e, \end{cases} \tag{8}$$

where S_e is the set of edge voxels, and $d(\mathbf{x}_i, \mathbf{x}_j)$ is the Euclidean distance between the two voxels $\mathbf{x}_i$ and $\mathbf{x}_j$.

4.3 Multipass Level Set Method

In many cases, we cannot obtain a sufficiently accurate classifier from the initial training samples extracted from the user-drawn boxes. Therefore, we have developed an EM-based method that improves the performance of both the voxel classifier and the level set method over multiple passes. The voxel classifier is re-trained at the end of every pass, and the training data is obtained from the latest segmentation result generated by the level set method. The re-trained classifier automatically generates an improved initialization for the level set method in the subsequent pass. Thus the multipass scheme is robust to initial user interactions and capable of gradually improving the result. Some intermediate results of our multipass level set method are shown in Fig. 4. It is evident that the summation of the classifier and edge field energy terms drops quickly over multiple passes.

[1] d_{max} is (Image Width + Image Height + Image Length)/8

5 EXPERIMENTAL RESULTS

We have implemented our 3D multipass level set method on an Intel Xeon E5540 2.53GHz processor with 8GB RAM and successfully applied it to a group of volumetric medical images, the Visible Human dataset. We use the Visualization Toolkit (Schroeder et al., 2004) to display the 3D segmentation results. The time for processing one 2D slice with resolution 640×480 is 5-8 seconds. Since such computation is performed independently over every pixel, the overall performance of our method can be significantly improved by parallelization on GPU of multi-cores. The computational time for each pass is less than 5 minutes. In the level set speed (2), $\alpha = 0.6$, $\beta = 0.6$, and $\gamma = 0.25$ during a regular pass. We apply 54 Gabor filters at 3 orientations and 2 scales at every pixel on 3 planes in 3 color-channels respectively. In (7), we always set $\mu = 0.5$. All the experiments were performed on color volume images. We have tested segmentation performance on multiple regions (abdomen, brain and hand) of the human body.

5.1 Segmentation of the Visible Human Dataset

We used a volume dataset with resolution $190 \times 344 \times 425$ to segment the spine, liver, kidney and intestine. The four segmentations were executed independently and the results are shown in Fig. 5. There are about 10 user-supplied boxes to

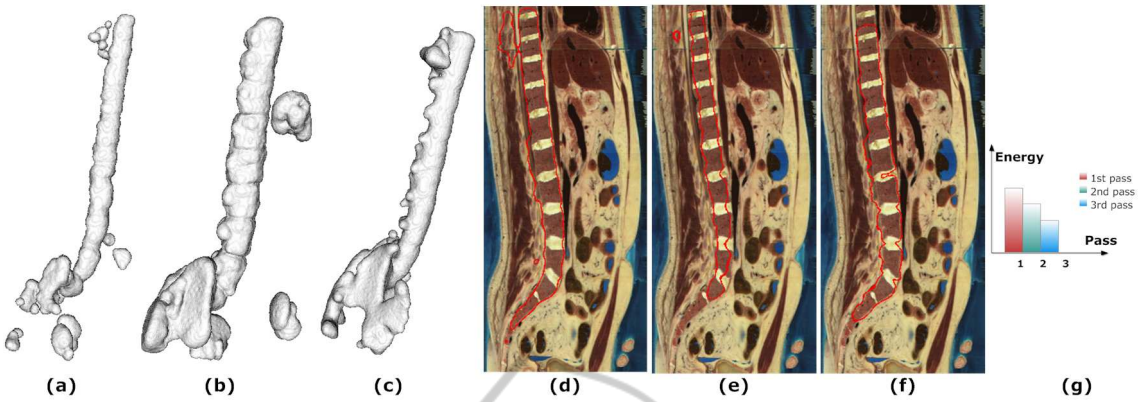

Figure 4: Multipass segmentation. Shown are the segmentation results after (a) the first pass, (b) the second pass, and (c) the third pass. (d)-(f) Contour of the zero level set (red) after the first pass, the second pass, and the third pass, respectively. (g) Classifier and edge field energy after each pass.

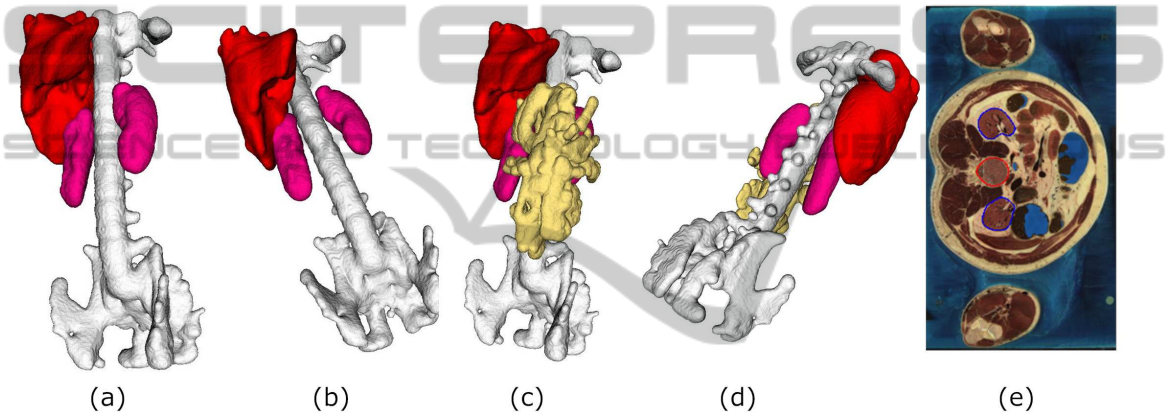

Figure 5: Segmentation in the abdomen area. (a)-(d) 3D visualization of segmented organs in the abdomen, including spine (white), liver (red), kidney (pink), and intestine (yellow). (e) Final contours of the zero level sets in a 2D slice (red for spine, blue for kidney).

roughly indicate which regions belong to the objects of interest and which belong to the background. The segmentation of liver is most challenging because its texture is very similar to the texture of muscle tissues. Our classifier and Gabor filter responses can successfully distinguish them as shown in Fig. 7.

5.2 Fiber Bundle Segmentation in Diffusion Tensor Images

Fiber bundles are coherently organized brain white matter pathways, which can be computed from diffusion tensor images. Our pipeline for fiber bundle segmentation includes the following stages: initial user input, classification on a 2D slice, (backward) fiber tracking and levelset-based fiber bundle extraction, as shown in Fig. 6. At the beginning, the user chooses a 2D image slice SL and draws a region of interest on it. A probabilistic classifier is then trained and used to assign probabilities to every voxel on the slice. During backward fiber tracking, we start fiber tracking from every voxel with fractional anisotropy greater than 0.1. If the fiber eventually passes a voxel p_{sl} on slice SL, we propagate the probability at p_{sl} to the voxel. We adopt the adaptive fourth order Runge-Kutta method as in (Press et al., 2002; Mori and van Zijl, 2002) to track fiber bundles. During the final stage, we run our levelset-based segmentation on the entire diffusion tensor image, whose voxels have been associated with probabilities, to finalize fiber bundle extraction.

Fig. 6 shows an example of fiber bundle segmentation. We extract *corpus callosum* from a volumetric diffusion tensor image using our level set method. *Corpus callosum* is a bridge between the left brain and the right one. It is filled with dense fibers (Aboitiz et al., 1992; Basser et al., 2000). The original data is a $256\times256\times32$ diffusion tensor image. The user first selects a 2D image slice near *corpus callosum*,

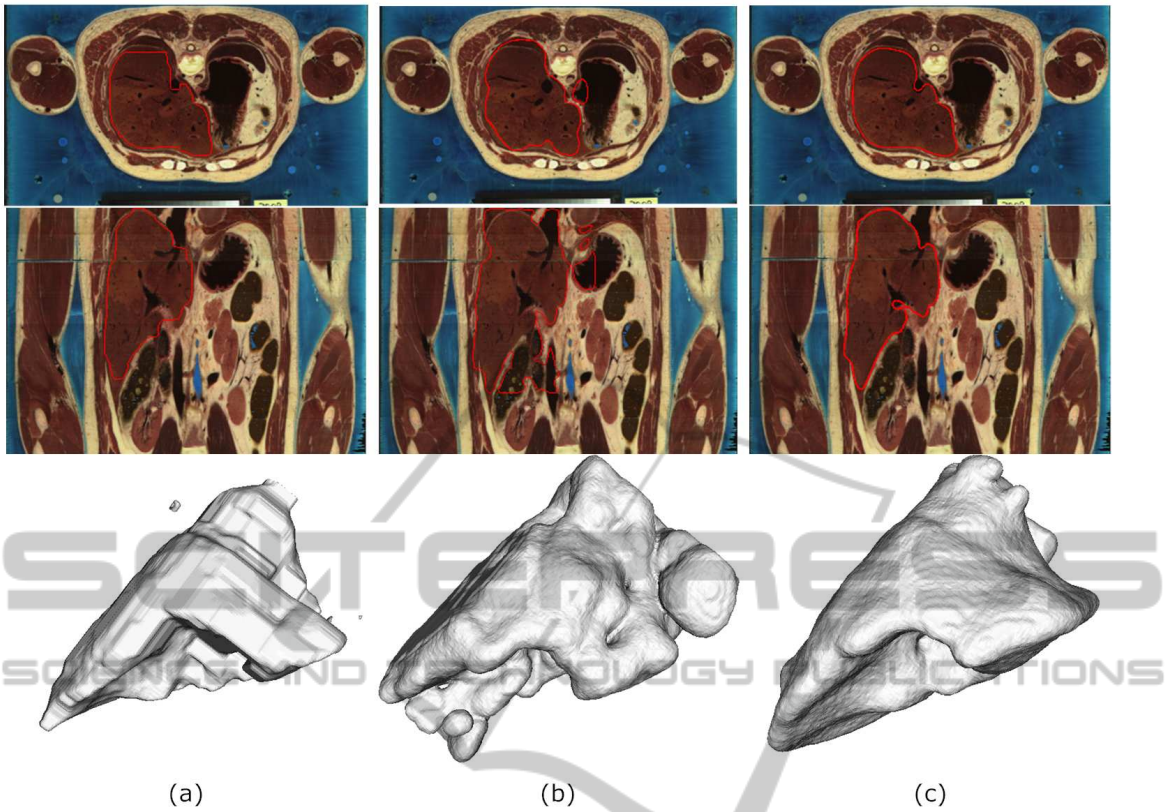

Figure 7: Segmentation Comparison. The first and second rows show segmentation results in 2D slices; the third row shows segmentation results using 3D visualization. (a) Graphcut, (b) the algorithm from (Holtzman-Gazit et al., 2006), (c) our method.

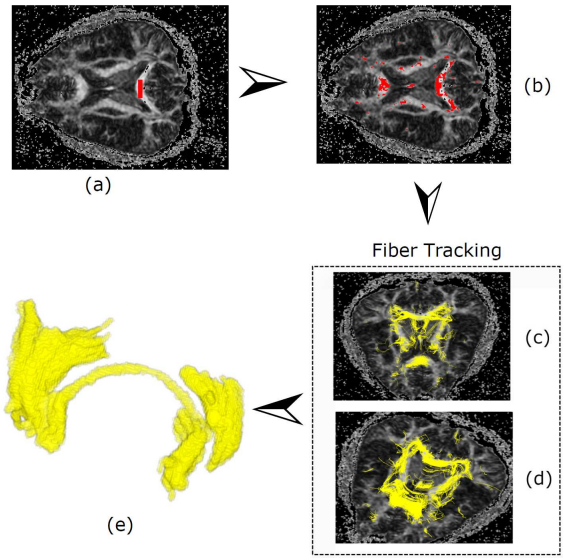

Figure 6: The pipeline of fiber bundle segmentation. (a) User-drawn region on a 2D slice of a diffusion tensor image, (b)initial foreground pixels chosen by the probabilistic classifier, (c)-(d) fiber tracking, (e) fiber bundles of corpus callosum segmented using our levelset-based method.

and draws two small rectangular regions on the slice. The entire fiber bundle can then be extracted using our method.

5.3 Comparisons

The level set method is a popular method in biomedical image segmentation (Holtzman-Gazit et al., 2006). We compared our segmentation algorithm with the popular graphcut algorithm (Boykov and Jolly, 2001) and another state-of-the-art levelset-based algorithm in (Holtzman-Gazit et al., 2006). The results are shown in Fig. 7. Minimization of the graphcut energy function gives rise to faceted segmentation boundaries, that do not accurately snap to salient volume edges. Note that we also integrated the same classifier with the graphcut algorithm. Even though the graphcut segmentation result (Fig. 7(a)) significantly overlaps with our segmentation result (Fig. 7(c)), the result from our method is much more accurate in boundary localization and also much smoother.

The levelset based method in (Holtzman-Gazit et al., 2006) is good at processing medical volume

images with thin structures. However, without the use of discriminative classifiers and texture descriptors, it could not distinguish liver tissues from muscle tissues, as shown in Fig. 7(b).

6 CONCLUSIONS

We have presented a robust and accurate method for biomedical image segmentation using level sets of probabilities. Our method integrates a probabilistic classifier with the level set method, making the level set method less vulnerable to local minima. Our method obtains a posterior probabilistic mask of an object of interest as the segmentation result. We further alternate classifier training and the level set method to improve the performance of both. We have successfully applied our method to the segmentation of various organs and tissues in the Visible Human dataset. Level sets of probabilities can be applied in segmentation of three dimensional MR images as shown in Fig. 6. Experiments and comparisons have demonstrated the effectiveness of our method.

ACKNOWLEDGMENTS

This work was partially supported by National Natural Science Foundation of China (NSFC) (61202255).

REFERENCES

Aboitiz, F., Scheibel, A. B., Fisher, R. S., and Zaidel, E. (1992). Fiber composition of the human corpus callosum. *Brain Research*, 598(1-2):143–153.

Basser, P. J., Pajevic, S., Pierpaoli, C., Duda, J., and Aldroubi, A. (2000). In vivo fiber tractography using dt-mri data. *Magnetic Resonance in Medicine*, 44:354–363.

Boykov, Y. and Jolly, M. (2001). Interactive graph cuts for optimal boundary and region segmentation of objects in n-d images. In *Intl. Conf. Computer Vision*, volume I, pages 105–112.

Cobzas, D., Birkbeck, N., Schmidt, M., and Jagersand, M. (2007). 3d variational brain tumor segmentation using a high dimensional feature set. In *Proceedings of the International Conference on Computer Vision*, pages 1–8. IEEE.

Friedman, J., Hastie, T., and Tibshirani, R. (2000). Additive logistic regression: a statistical view of boosting. *The Annals of Statistics*, 28(2):337–407.

Hadwiger, M., Kniss, J. M., Rezk-salama, C., Weiskopf, D., and Engel, K. (2006). *Real-time Volume Graphics*. A. K. Peters, first edition.

Holtzman-Gazit, M., Kimmel, R., Peled, N., and Goldsher, D. (2006). Segmentation of thin structures in volumetric medical images. *IEEE Transaction on Image Processing*, 15(2):354–363.

Liu, Y. and Yu, Y. (2012). Interactive image segmentation based on level sets of probabilities. *IEEE Transaction on Visualization and Computer Graphics*, 18(2):202–213.

Manjunath, B. and Ma, W. (1996). Texture features for browsing and retrieval of image data. *IEEE Transactions on Pattern Analysis and Machine Intelligence*, 18(8):837–842.

Mori, S. and van Zijl, P. C. M. (2002). Fiber tracking: principles and strategies - a technical review. *NMR IN BIOMEDICINE*, 15:468–480.

Osher, S. J. and Fedkiw, R. P. (2003). *Level Set Methods and Dynamic Implicit Surfaces*. Springer-Verlag, first edition.

Paragios, N. and Deriche, R. (1999). Geodesic active regions for supervised texture segmentation. In *Proceedings of the International Conference on Computer Vision*, volume 2, pages 926–932. IEEE.

Peng, D., Merriman, B., Osher, S., Zhao, H., and Kang, M. (1999). A pde-based fast local level set method. *Journal of Computational Physics*, 155(2):410–438.

Pham, D. L., Xu, C., and Prince, J. L. (2000). Current methods in medical image segmentation. *Annual Review of Biomedical Engineering*, 2:315–337.

Press, W. H., Saul A. Teukolsky, W. T. V., and Flannery, B. P. (2002). *Numerical recipes in C++: the art of scientific computing*. Cambridge University Press,New York, second edition.

Schroeder, W., Martin, K., and Lorensen, B. (2004). *The Visualization Toolkit*. Kitware Inc., third edition.

Sethian, J. (1999). *Level Set Methods and Fast Marching Methods*. Cambridge University Press.

Tu, Z., Narr, K. L., Dollar, P., Dinov, I., Thompson, P. M., and Toga, A. W. (2008). Brain anatomical structure segmentation by hybrid discriminative/generative models. *IEEE Transactions on Medical Imaging*, 27(4):495–508.